

Theoretical study of the rovibrationally resolved transitions of CaH

P. F. Weck^{a)} and P. C. Stancil^{b)}

Department of Physics & Astronomy and Center for Simulational Physics, The University of Georgia, Athens, Georgia 30602-2451

K. Kirby^{c)}

Institute for Theoretical Atomic, Molecular and Optical Physics, Harvard-Smithsonian Center for Astrophysics, Cambridge, Massachusetts 02138

(Received 15 January 2003; accepted 18 March 2003)

Comprehensive absorption line lists for ^{40}CaH have been calculated for electronic transitions from the $X^2\Sigma^+$ ground state to the $A^2\Pi$, $B/B'^2\Sigma^+$, and $E^2\Pi$ low-lying excited states. The lists include transition energies and oscillator strengths for all possible allowed transitions and were computed using the most recent set of theoretical potential energy curves and dipole transition moment functions, with adjustments to account for experimental dissociation energies and asymptotic limits. Good agreement with previous calculations and available experimental data has been obtained. Oscillator strengths for the transition from the $X^2\Sigma^+$ state to the $D^2\Sigma^+$ state are also given, but due to the large uncertainty of the available dipole transition moment function the line list is highly uncertain. For the $C^2\Sigma^+ \leftarrow X^2\Sigma^+$ transition, a Franck–Condon approximation has been used. © 2003 American Institute of Physics. [DOI: 10.1063/1.1573181]

I. INTRODUCTION

Metal hydrides play an important role in various areas of astrophysics. Indeed, their spectra appear in such diverse environments as in sun spots or in dense molecular clouds of the interstellar medium, where they are thought in the latter to be a significant repository of gas-phase metals.¹ They are also frequently found with relatively large abundances in cool stellar atmospheres (M and later types), where molecular absorption is the most important opacity source.²

However, the lack of accurate and complete molecular absorption line lists for a large number of metal hydrides has been a serious limitation to developing reliable atmospheric models of cool stars and extrasolar giant planets. These models are important for producing synthetic spectra which can be used in comparisons with observations to deduce relevant physical parameters, such as surface chemical composition and effective temperature.

In this work, we focus on improving the molecular absorption line lists for calcium monohydride, for which only limited data are available.³ Although the low-lying vibrational and rotational energy levels of the first several electronic states of CaH were investigated in the first half of the 20th century, a more complete picture of the electronic structure and spectroscopy of this molecule has only emerged from numerous recent experimental and theoretical studies.^{3–9} The spectrum of CaH is characterized by strong perturbations of various types, from local shifts to large interactions between electronic states. The most illustrative examples of such perturbations are found for the transitions to the $B/B'^2\Sigma^+$ asymmetric double-well and to the $D^2\Sigma^+$

electronic state, which both show avoided crossings in the adiabatic picture.

We present comprehensive and extensive theoretical line lists for ^{40}CaH for the electronic transitions from the $X^2\Sigma^+$ ground state to the $A^2\Pi$, $B^2\Sigma^+$, and $E^2\Pi$ excited states. The lists contain the transition energies and oscillator strengths for allowed rotational and vibrational transitions. Oscillator strengths for the $D^2\Sigma^+ \leftarrow X^2\Sigma^+$ transition have also been calculated, but the resulting line list is highly uncertain due to the large uncertainty of the corresponding dipole transition moment function. The Franck–Condon approximation has been used for the $C^2\Sigma^+ \leftarrow X^2\Sigma^+$ transition. Atomic units are used throughout unless otherwise stated.

II. MOLECULAR THEORY

A. Potential energy curves and dipole transition moments

The *ab initio* potential curves and dipole transition moments calculated by Leininger and Jeung³ have been used in the present work for transitions from the $X^2\Sigma^+$ electronic ground state to the $A^2\Pi$, $B^2\Sigma^+$, $C^2\Sigma^+$, $D^2\Sigma^+$, and $E^2\Pi$ excited states. Starting from an all-electron restricted Hartree–Fock calculation using a large Gaussian-type basis set, they constructed configuration interaction (CI) wave functions, including all possible single and double excitations. The spectroscopic constants derived from these calculations reproduce experimental data within the experimental uncertainty.

1. Potential energy curves

Potential energy curves were obtained by Leininger and Jeung³ over a range of internuclear distances $R=2.75a_0$ to $9.0a_0$. Though results for the $C^2\Sigma^+$ state were obtained over this range, no data were reported in the vicinity of R

^{a)}Electronic mail: weck@physast.uga.edu

^{b)}Electronic mail: stancil@physast.uga.edu

^{c)}Electronic mail: kirby@cfa.harvard.edu

TABLE I. Asymptotic separated-atom and united-atom limits for CaH.

Molecular state	Separated atom				United atom (Sc)	
	Atomic states	Energy (cm ⁻¹) ^a	C ₆ ^b	C ₈ ^{b,d}		C ₁₀ ^{b,d}
X ² Σ ⁺	Ca(4s ² 1S)+H(² S)	0	119 ^c	6.51(3) ^c	3.35(5) ^c	Sc(3d4s ² 2D)
A ² Π	Ca(4s4p ³ P ⁰)+H(² S)	15 263.089	194	7.77(3)	5.46(5)	Sc(3d4s ² 2D)
B ² Σ ⁺	Ca(4s4p ³ P ⁰)+H(² S)	15 263.089	194	7.77(3)	5.46(5)	Sc(3d ² 4s ² F)
D ² Σ ⁺	Ca(3d4s ³ D)+H(² S)	20 356.625	83.3	3.34(3)	2.35(5)	Sc(3d ² 4s ² D)
E ² Π	Ca(3d4s ³ D)+H(² S)	20 356.625	83.3	3.34(3)	2.35(5)	Sc(3d ² 4s ² F)
C ² Σ ⁺	Ca(3d4s ¹ D)+H(² S)	21 849.634	35.7	1.43(3)	1.00(5)	Sc(3d ² 4s ² G)

^aWeighted average of the multiplet term energies from the NIST Atomic Spectra Database (1999).

^bEstimated except for the ground state values; see the text for details.

^cFrom Standard and Certain (Ref. 12).

^dNotation: $x(n) \equiv x \times 10^n$.

$\approx 5.0a_0$. In this work, the potential energy values calculated by Boutalib *et al.*⁸ for this electronic state have been used over the range $R = 5.0a_0$ to $9.0a_0$. A shift of $+0.26a_0$ of this potential curve over the internuclear separation range of interest was required in order to obtain the same adiabatic internuclear equilibrium distance, $R_e(C^2\Sigma^+) = 3.72a_0$, as calculated in Ref. 3.

Shifts in energy have been applied in the present work to the calculated potential curves in order to bring them into agreement with the dissociation energies D_0^0 from experiment or estimated values. The dissociation energy adopted here for the electronic ground state $X^2\Sigma^+$ was $13\,776\text{ cm}^{-1}$, according to the experimental value given by Huber and Herzberg.¹⁰ As no experimental data are available for the excited states, dissociation energies were calculated by use of the separated-atom asymptote values given in Table I, the experimental dissociation energy of the $X^2\Sigma^+$ state, and the observed pure vibronic transition energies, ν_{00} .¹⁰ Separated-atom energies have been calculated using a weighted average of the multiplet term energies from the NIST Atomic Spectra Database.¹¹ The dissociation energies, energy shifts to the *ab initio* potential curves, and ν_{00} vibronic transitions are given in Table II. The relative energies between the potential curves of the electronic ground state and the excited states were further shifted to match the energy differences corresponding to the experimental vibronic transitions ν_{00} .

Beyond the range of internuclear separations $R = 2.75a_0$ to $9.0a_0$ considered by Leininger and Jeung,³ the potential-energy curves have been extrapolated in two different ways. For internuclear distances $R > 9.0a_0$, a smooth fit to the *ab initio* potentials has been performed using the dispersion potential expansion

$$V(R) = -\frac{C_6}{R^6} - \frac{C_8}{R^8} - \frac{C_{10}}{R^{10}}, \quad (1)$$

where C_6 , C_8 , and C_{10} are the usual van der Waals coefficients corresponding to the dipole–dipole, dipole–quadrupole, and the sum of quadrupole–quadrupole and dipole–octupole interactions, respectively. For the $X^2\Sigma^+$ electronic state, the lower bounds to the van der Waals coefficients given by Standard and Certain¹² were adopted.

Since, to our knowledge, no data have been reported for the van der Waals coefficients of the excited states of CaH, we estimate them using various versions of the London formula for C_6 as described by Dalgarno and Kingston.¹³ We consider four relations. The two simplest involve only the ionization energies and static dipole polarizabilities, α , of the ground state of H and the excited state of Ca. The two other expressions for C_6 require either: (1) a summation over oscillator strengths and transition energies for all allowed transitions of both H and Ca; or (2) a similar summation for the allowed transitions of Ca with the influence of H being introduced only through α . The sum includes both discrete and continuum transitions, but we consider here only discrete transitions with the oscillator strengths and transition energies taken from the experimental compilation of Ref. 11. The latter relations appear to underestimate C_6 when compared to more rigorous calculations, while the former two overestimate it, with the dispersion being typically a factor of 2. We therefore compute C_6 using all four expressions and take the average. For the case of ground state Ca and H, this procedure gives $C_6 = 105$ a.u. compared to the range of 119–123 a.u. obtained by Standard and Certain.¹² Therefore, the C_6 's calculated here are expected to be underestimates (due to the neglect of continuum transitions), but reliable to within $\sim 30\%$.

For the dipole polarizabilities of Ca, the values computed by Mérawa, Tendero, and Rérat¹⁴ are adopted for the S and P states: $4s^2\,^1S$ (163.0 a.u.), $4s5s\,^1S$ (2963), $4s5s\,^3S$

TABLE II. Dissociation energies D_0^0 , vibronic transition energies ν_{00} , and energy shifts (in cm⁻¹).

Molecular state	X ² Σ ⁺	A ² Π	B ² Σ ⁺	E ² Π	D ² Σ ⁺	C ² Σ ⁺
D_0^0	13 776 ^a	14 608.7 ^b	13 284.2 ^b	13 740.6 ^b	11 608.6 ^b	7 277.6 ^b
ν_{00} ^a	...	14 430.4	15 754.9	20 392	22 524	28 348
Energy shift	-707.1	-641.9	-1 163.0	-1 389.9	-779.6	-172.0

^aFrom Huber and Herzberg (Ref. 10).

^bCalculated from the separated-atom energies of Table I and the ν_{00} values of Ref. 10.

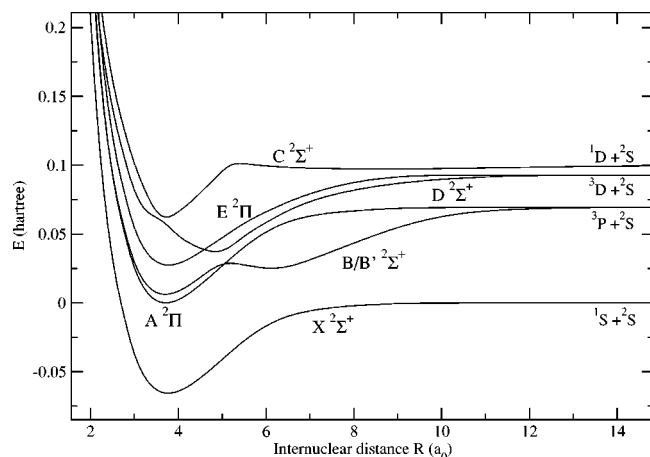


FIG. 1. Potential energy curves of the $X^2\Sigma^+$ ground state and the $A^2\Pi$, $B^2\Sigma^+$, $C^2\Sigma^+$, $D^2\Sigma^+$, and $E^2\Pi$ excited states of CaH.

(1940), $4s4p^1P^0$ (55.3), and $4s4p^3P^0$ (276). From the sum of the discrete oscillator strengths, we obtain: $4s^2^1S$ (155 a.u.), $4s5s^1S$ (3364), $4s5s^3S$ (2001), $4s4p^1P^0$ (163), and $4s4p^3P^0$ (231). The value for the $^1P^0$ calculated by Mérawa, Tendero, and Rérat¹⁴ appears to be incorrect due to the neglect of some strong transitions which are experimentally observed, so that our larger value is to be preferred. The close agreement of most of the polarizabilities suggests that the continuum contribution is not significant, except for the $^3P^0$, where it appears to be about 20%. The general agreement also suggests that for the C_6 calculations, the explicit sums of oscillator strengths have accounted for the majority of the transitions. For the D state, for which no previous data exist, we estimate the dipole polarizabilities to be 73.9 and 173 a.u. for $3d4s^1D$ and $3d4s^3D$, respectively.

The C_8 and C_{10} coefficients were not computed, but estimated by scaling the $X^2\Sigma^+$ values by the ratio of the excited state C_6 to the ground state C_6 . The reliability of this procedure is unknown, but the long-range potential is dominated by the C_6 term. The adopted van der Waals coefficients, summarized in Table I, should allow for a reasonable determination of the energy and number of the highest-lying rovibrational states.

For internuclear distances $R < 2.75a_0$, the potential curves of all the electronic states have been fitted to the short-range interaction exponential form $A \exp(-BR) + C$. The potential energy curves used in the current calculations are shown in Fig. 1.

2. Dipole transition moments

The dipole transition moments of Leininger and Jeung³ and Leininger,¹⁵ which were computed over the internuclear distance interval $2.75 \leq R \leq 10a_0$, were adopted in this work and are presented in Fig. 2. These are the only available transition moment functions in the literature; however, close examination reveals a number of problems. First, no information on the relative signs of the transition moments is available; i.e., they are all given as positive quantities. Given the large number of crossings and avoided crossings of the molecular potential curves, one would expect some sign

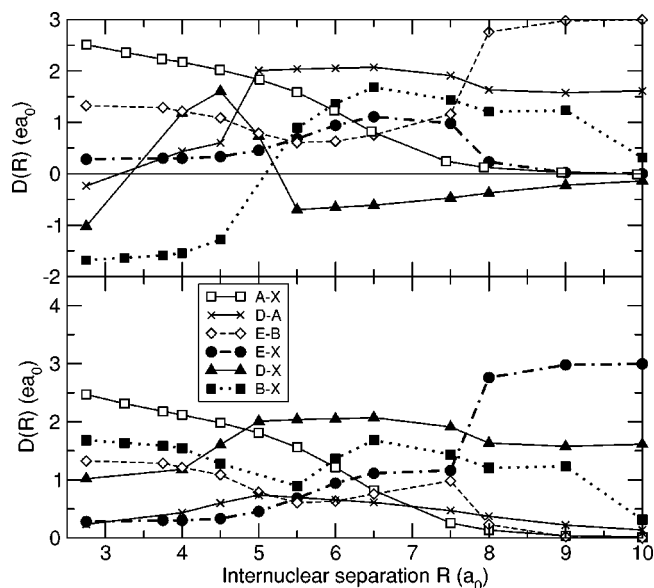


FIG. 2. Dipole transition moment functions for CaH. Top: functions used in the present work. Bottom: original functions calculated by Leininger and Jeung (Ref. 3) and Leininger (Ref. 15).

changes to occur in the dipole moment functions as the internuclear separation changes. Second, many of the transition moments appear not to go to the correct separated-atom limits, as can be ascertained by consulting Table I. While recognizing that the best solution would be to perform new molecular structure calculations, we shall instead make reasonable adjustments, on physical grounds, to the transition moment functions given in Refs. 3 and 15. This approach is certainly better than adopting the Franck–Condon approximation (i.e., unity for all transition moments) and, we will attempt to demonstrate below, an improvement over the raw transition moment functions as given in Ref. 15.

We first consider transition moments amongst the $X^2\Sigma^+$, $A^2\Pi$, and $B^2\Sigma^+$ states in analogy with those of the chemically similar alkaline–earth hydride MgH as calculated by Saxon *et al.*¹⁶ The $A \leftarrow X$ transition moment is smooth, has no sign change, and its behavior is similar to the same transition in MgH. We therefore accept it as given in Ref. 3. However, the $B \leftarrow X$ transition moment displays, as given in Leininger and Jeung,³ an abrupt slope reversal near $R = 5a_0$. This internuclear distance is the location of an avoided-crossing of the B state with the $X^2\Sigma^+$ ($R = 4.5a_0$) and $D^2\Sigma^+$ ($R = 5.0a_0$). Further, the dipole moments of the B and D states, calculated by Leininger and Jeung,³ cross near $R = 5a_0$. Martin⁶ finds a similar crossing from a semi-quantitative analysis of the electron charge density. Therefore, a negative sign is adopted for the $B \leftarrow X$ transition moment for $R < 5a_0$. A similar sign change occurs for MgH.¹⁶

Of major concern is the observation that by $R = 10a_0$, the $D \leftarrow X$, $E \leftarrow X$, $D \leftarrow A$, and $E \leftarrow B$ transition moments, as given by Leininger,¹⁵ are not approaching the correct separated-atom limits. The former two cases correspond to intercombination Ca transitions which should be zero in a nonrelativistic approximation, while the latter two should approach the Ca ($^3P - ^3D$) transition moment, which is non-zero. The reverse behavior is observed in Fig. 2. For the

$E \leftarrow X$ and $E \leftarrow B$ transitions, the situation is rectified by interchanging the transition moments for $R > 7.5a_0$, thus forcing them to go to the correct separated-atom limits. $R = 7.5a_0$ is chosen as the two transition moments approach each other at this internuclear separation and then diverge. For the $D \leftarrow X$ transition, two sign changes are expected since the $D^2\Sigma^+$ exhibits a first avoided crossing with the $C^2\Sigma^+$ state at $R = 3.6a_0$ followed by a second one with the $B^2\Sigma^+$ as previously mentioned. Consequently, a sign change is made at $R = 2.75a_0$ for the $D \leftarrow X$ transition. Then, switching the $D \leftarrow X$ and $D \leftarrow A$ dipole transition moments for $R \geq 5a_0$ and changing the phase of the $D \leftarrow X$ for $R \geq 5.5a_0$ enables the two transition moments to approach the correct asymptotic limits. We believe that the resulting dipole transition moments, presented in Fig. 2, are a better representation of the true values as they take into account the correct separated-atom limits and the behavior of the crossings and avoided crossings of the molecular terms. For $R < 2.75a_0$ and $R > 10a_0$, the dipole transition moments were extrapolated by exponential fits and smoothly forced to the correct united-atom and separated-atom limits.

For the $C \leftarrow X$ transition, no values of the corresponding dipole transition moment function are available. Consequently, we use the Franck–Condon approximation. Future molecular structure calculations may show this to be a poor approximation as there are two avoided crossings of the C state, one with the D state at $R = 3.6a_0$ and one with the higher-lying $K^2\Sigma^+$ near $R = 5.5a_0$, implying two significant changes of character in the wave function as a function of R .

B. Rotational oscillator strengths

Throughout the present study, we have adopted the expression of Whiting and Nicholls¹⁷ for the calculation of vibrational, rotational line oscillator strengths.

For a discrete absorption transition to a given bound rovibrational state $v'N'$ of the final electronic state from a rovibrational state $v''N''$ of the initial electronic state, the rotational oscillator strength can be expressed by¹⁸

$$f_{v'N',v''N''}^{ab} = \frac{2}{3} \Delta E_{v'N',v''N''} \frac{S_{N'}(N'')}{2N''+1} |D_{v'N',v''N''}|^2, \quad (2)$$

where $\Delta E_{v'N',v''N''}$ is the absorbed photon energy, and $D_{v'N',v''N''} = \langle \chi_{v'N'} | D(R) | \chi_{v''N''} \rangle$ is the rovibrational matrix element of the electric dipole transition moment $D(R)$, responsible for transitions between the initial and final electronic states. The rovibrational wave functions $\chi_{vN}(R)$ are solutions of the radial nuclear Schrödinger equation

$$\left[-\frac{1}{2\mu} \frac{d^2}{dR^2} + E_{\text{el}}(R) + \frac{N(N+1) - \Lambda^2}{2\mu R^2} - E_{vN} \right] \chi_{vN}(R) = 0, \quad (3)$$

where μ is the reduced mass of the system, N is the rotational quantum number corresponding to the angular momentum of nuclear rotation neglecting the nuclear and electronic spins, Λ is the projection of the electronic angular

momentum onto the molecular axis, and $E_{\text{el}}(R)$ and E_{vN} are the electronic potential energy and rovibrational energy eigenvalues, respectively.

The Hönl–London factors, $S_{N'}(N'')$ of Eq. (2), are defined according to Ref. 17 as follows:

for a $\Sigma \leftarrow \Sigma$ electronic transition

$$S_{N'}(N'') = \begin{cases} N'', & N' = N'' - 1 \text{ (P branch)} \\ N'' + 1, & N' = N'' + 1 \text{ (R branch)}, \end{cases} \quad (4)$$

and for a $\Pi \leftarrow \Sigma$ transition,

$$S_{N'}(N'') = \begin{cases} (N'' - 1)/2, & N' = N'' - 1 \text{ (P branch)} \\ (2N'' + 1)/2, & N' = N'' \text{ (Q branch)} \\ (N'' + 2)/2, & N' = N'' + 1 \text{ (R branch)}. \end{cases} \quad (5)$$

For the sake of comparison with the band oscillator strength values calculated by Leininger and Jeung,³ we used the following relation between band and rotational oscillator strengths, as defined in Eq. (2):

$$f_{v'v''}^{ab} = \frac{g_{N',N''}^{ab}}{S_{N'}(N'')} f_{v'N',v''N''}^{ab} = \frac{(2 - \delta_{0,\Lambda''+\Lambda'}) (2N'' + 1)}{(2 - \delta_{0,\Lambda''}) S_{N'}(N'')} f_{v'N',v''N''}^{ab}, \quad (6)$$

where $g_{N',N''}^{ab}$ is a degeneracy factor arising from spin splitting and Λ -doubling in both final and initial electronic states, effects which are neglected in this work.

III. RESULTS AND DISCUSSION

The energy levels and rovibrational wave functions $\chi_{v'N'}(R)$ and $\chi_{v''N''}(R)$ of the final and initial electronic states were calculated by solving the radial nuclear equation (3) by standard Numerov techniques.¹⁹ Calculations were performed on a grid with a step size of $1 \times 10^{-3}a_0$ for the integration over internuclear distances from $R = 0.5a_0$ to $200a_0$. The reduced mass $\mu = 0.983\,033\,88\text{ u}$ (Ref. 27) = 3585.0092 a.u. (Ref. 10) was chosen for ^{40}CaH . For the asymmetric double-well potential $B/B'^2\Sigma^+$, the radial nuclear equation was solved by use of the LEVEL 7.5 code developed by Le Roy.²⁰

In Tables III and IV, the calculated energy differences between consecutive rotationless vibrational levels, $\Delta G(v+1/2) = G(v+1) - G(v)$, are given for the $X^2\Sigma^+$, $A^2\Pi$, $B^2\Sigma^+$, and $D^2\Sigma^+$ states. Experimental values^{5,21,22} are also displayed together with the results, for the $X^2\Sigma^+$ and $B/B'^2\Sigma^+$ states, calculated by Martin⁶ using a semiempirical model. The theoretical results of Carlsund-Levin *et al.*²³ obtained by use of an exterior complex rotated coupled channel description are also shown for comparison for the $B/B'^2\Sigma^+$ and $D^2\Sigma^+$ states. For the $X^2\Sigma^+$, our calculations agree with experiment within less than 1%. The discrepancies arise mainly from the use of the somewhat too broad ground state potential of Leininger and Jeung,³ as suggested by the narrower spacings of the vibrational levels for our theoretical results. Moreover, from our energy shifting pro-

TABLE III. $\Delta G(v+1/2)$ in cm^{-1} and maximum rotational quantum number N_{max} for the $X^2\Sigma^+$ and $A^2\Pi$ states.

v	$X^2\Sigma^+$				$A^2\Pi$	
	N_{max}^a	Theory ^a	Martin ^b	Expt. ^c	N_{max}^a	Theory ^a
0	61	1248.1	1261.2	1260.1	62	1284.4
1	58	1211.1	1221.2	1222.0	60	1244.2
2	56	1174.8	1183.7	1183.3	57	1200.8
3	53	1138.2	1147.8		55	1158.2
4	50	1101.2	1115		52	1119.2
5	48	1063.4	1083		50	1080.2
6	45	1020.3	1050		47	1037.8
7	42	969.3	1017		44	989.8
8	39	910.5	982		41	935.3
9	36	843.9	943		38	874.4
10	32	766.4	900		35	805.9
11	29	671.6	846		32	725.0
12	26	557.7	777		29	626.6
13	22	445.3			25	512.0
14	18	339.4			22	397.7
15	13	235.1			18	301.8
16	7				14	222.8
17					8	

^aThis work.^bMartin (Ref. 6).^cReferences 5, 21, and 22.

cedure and from the long-range expansion of the dispersion potential, three additional vibrational levels have been found for this electronic state with respect to the 14 levels calculated in Ref. 6. Our theoretical predictions for the $B/B'^2\Sigma^+$ state are in excellent agreement with the available experimental data, with a maximum difference of 3.4 cm^{-1} for $\Delta G(3/2)$. Similar to the previous calculations of Martin,⁶ the double-well character of the B/B' electronic state is manifested by strong perturbations, starting from $v=3$, in the ΔG progression. While there is a good agreement for the ΔG for $v < 3$ among all of the theoretical results, there are significant discrepancies for larger v . Experimental data which could provide some discrimination are lacking. A total of 29 vibrational levels has been found for this state with six more levels than obtained in Ref. 6 and three more than found in Ref. 23.

We are unaware of any experimental data for the ΔG progression of $D^2\Sigma^+$, but there is a reasonable agreement between the current calculations and those of Refs. 6 and 23 for $v < 3$. For larger v , the discrepancies are probably due to differences in the adopted potential curves. Neither experimental nor theoretical data on the vibrational spacings for the A , C , and E states appear to be available.

TABLE IV. $\Delta G(v+1/2)$ in cm^{-1} and maximum rotational quantum number N_{max} for the $D^2\Sigma^+$ and $B/B'^2\Sigma^+$ states.

v	$D^2\Sigma^+$				$B/B'^2\Sigma^+$				Expt. ^d
	N_{max}^a	Theory ^a	Martin ^b	Carlsund-Levin ^c	N_{max}^a	Theory ^a	Martin ^b	Carlsund-Levin ^c	
0	68	1089.8	1044	1027.03	109	1241.6	1248.2	1249.14	1244.4
1	65	999.9	968	999.76	29	1189.2	1188.7	1192.21	1192.6
2	62	928.6	920	957.98	97	1109.1	1094.5	1109.90	
3	60	853.4	888	918.02	29	322.1	526	518.88	
4	57	774.9	860	881.58	29	491.6	332	347.84	
5	55	703.2	837	859.00	84	243.9	356	323.49	
6	52	648.8	813	851.30	80	453.3	466	453.65	
7	50	622.2	789	827.70	76	441.1	482	479.09	
8	47	600.6	766	800.83	72	450.0	499	477.65	
9	45	572.8	741	772.91	68	466.0	520	634.79	
10	43	537.5	716	622.03	65	467.5	528	409.17	
11	40	497.7		435.74	63	469.1	534	650.93	
12	38	456.6		689.55	61	471.0	534	413.00	
13	35	417.0		661.21	59	473.2	533	614.36	
14	33	379.8		623.13	57	473.1	526	436.85	
15	30	342.8		582.95	55	467.6	518	571.11	
16	27	306.0		540.66	53	456.8	506	445.96	
17	24	269.3		497.10	51	444.1	491	524.62	
18	21	232.5		454.77	48	427.9	473	440.58	
19	17	193.2		417.49	46	407.2	450	462.76	
20	12				43	384.4	423	415.05	
21					41	357.2	389	386.04	
22					38	327.3	343	339.84	
23					35	293.8		209.10	
24					32	257.4		32.97	
25					29	218.4		56.98	
26					26	177.2			
27					22	134.8			
28					18	92.7			
29					14				

^aThis work.^bMartin (Ref. 6).^cCarlsund-Levin *et al.* (Ref. 23).^dReferences 5, 21, and 22.

TABLE V. Band oscillator strengths for the $A^2\Pi\leftarrow X^2\Sigma^+$ and $B/B'^2\Sigma^+\leftarrow X^2\Sigma^+$ systems. Band oscillator strengths are calculated in this work from line oscillator strengths, according to Eq. (6), with rotational quantum numbers $N''=0$ and $N'=0$ (Q branch) for $\Pi\leftarrow\Sigma$ transitions and $N''=0$ and $N'=1$ (R branch) for $\Sigma\leftarrow\Sigma$ transitions. Our results are listed on the first line, with the previous calculations of Ref. 3 below. Notation: $x(-n)\equiv x\times 10^{-n}$. A single dash means less than 0.0001.

v''/v'	0	1	2	3	4	5	6	7
$A\leftarrow X$								
0	2.037(-1) 2.054(-1)	2.2(-3) 2.2(-3)
1	4.1(-3) 4.2(-3)	1.942(-1) 1.957(-1)	4.0(-3) 4.1(-3)
2	1(-4) 1(-4)	7.8(-3) 7.8(-3)	1.851(-1) 1.865(-1)	5.5(-3) 5.5(-3)
3	...	4(-4) 4(-4)	1.11(-2) 1.10(-2)	1.765(-1) 1.778(-1)	6.2(-3) 6.3(-3)	1(-4) 1(-4)
4	8(-4) 8(-4)	1.30(-2) 1.32(-2)	1.684(-1) 1.698(-1)	6.6(-3) 6.6(-3)	2(-4) 2(-4)	...
5	1(-4) 1(-4)	1.2(-3) 1.2(-3)	1.48(-2) 1.50(-2)	1.604(-1) 1.618(-1)	6.5(-3) 6.5(-3)	4(-4) 4(-4)
6	1(-4) 1(-4)	1.6(-3) 1.6(-3)	1.64(-2) 1.64(-2)	1.520(-1) 1.535(-1)	6.2(-3) 6.2(-3)
7	2(-4) 2(-4)	2.1(-3) 2.1(-3)	1.78(-2) 1.78(-2)	1.427(-1) 1.442(-1)
$B/B'\leftarrow X$								
0	1.163(-1) 1.189(-1)	2.1(-3) 2.0(-3)
1	3.1(-3) 3.3(-3)	1.070(-1) 1.080(-1)	2.6(-3) 2.5(-3)	6(-4) 5(-4)
2	2(-4) 2(-4)	5.6(-3) 5.9(-3)	9.45(-2) 9.72(-2)	1.0(-3) 1.6(-3)	...	1.2(-3) 7(-4)	1.1(-3) 6(-4)	1(-4) 1(-4)
3	...	3(-4) 4(-4)	8.1(-3) 7.3(-3)	7.53(-2) 8.70(-2)	4(-4) 3(-4)	1.4(-3) 2(-4)	...	1.4(-3) 1.1(-3)
4	3(-4) 7(-4)	9.7(-3) 5.3(-3)	2(-4) 6(-4)	1.75(-2) 3.22(-2)	3.01(-2) 3.93(-2)	1.22(-2) 8.6(-3)
5	2(-4) 1(-4)	1(-4) 1.5(-3)	...	3.0(-3) 3(-4)	5.8(-3) 3.6(-3)	9.5(-3) 2.17(-2)
6	4(-4) ...	4(-4) 8(-4)	...	4(-4) ...	2.9(-3) 6(-4)
7	1(-4) ...	1.8(-3) 1.9(-3)	3.3(-3) 2.1(-3)	4(-4) 2.0(-3)	1.0(-3) 2.6(-3)

By means of Eq. (6), an estimate of the effects of our shifting procedure on the calculated line lists may be obtained by comparison with the theoretical band oscillator strength values obtained by Leininger and Jeung.³ The band oscillator strength for the band system $A^2\Pi\leftarrow X^2\Sigma^+$, for which the original dipole transition moment of Ref. 3 has been used, is given in Table V for the transitions between the vibrational states $v''=0-7$ and $v'=0-7$. Our band oscillator strengths have been derived from rotational transitions between levels with quantum numbers $N''=0$ and $N'=0$. The current calculations are found to be in excellent agreement with the previous theoretical results. The main discrepancies, of the order of 1% up to $v''=v'=7$, are observed for the $\Delta v=v'-v''=0$ vibronic transitions, the most intense bands of the $A\leftarrow X$ system. The discrepancies are primarily due to the adoption of the larger theoretical v_{00} by Leininger and Jeung.³

Our $B/B'\leftarrow X$ band oscillator strengths obtained from $N''=0\leftarrow N'=1$ rotational transitions are reported in Table V, for the vibrational states $v''=0-7$ and $v'=0-7$, and

compared to the theoretical results of Ref. 3. The band oscillator strength $f_{0,0}$ for the transition between both ground vibrational levels is found to be 0.116, in excellent agreement with the experimental estimate of 0.11 ± 0.005 given by Klynning *et al.*²⁴ The other band oscillator strengths are in good agreement with Leininger and Jeung.³ The discrepancies again result from the adoption of a smaller v_{00} in this work taken from experiment. For $v>2$, more significant differences can be noted, presumably due to our changing of the sign of the dipole transition moment for $R<5a_0$. However, as noted in Ref. 3, the double-well results in an atypical oscillator strength distribution, with the dominant transitions shifting away from $\Delta v=0$, for $v'\geq 4$.

While Leininger and Jeung³ do tabulate band oscillator strengths for the $D\leftarrow X$ transitions, the significant changes in the dipole transition moment proposed here make a comparison difficult. We are unaware of any band oscillator strength tabulations for the $C\leftarrow X$ and $E\leftarrow X$ transitions.

Figure 3 shows the line absorption rotational oscillator strengths²⁵ for the $A^2\Pi\leftarrow X^2\Sigma^+$ transition as a function of

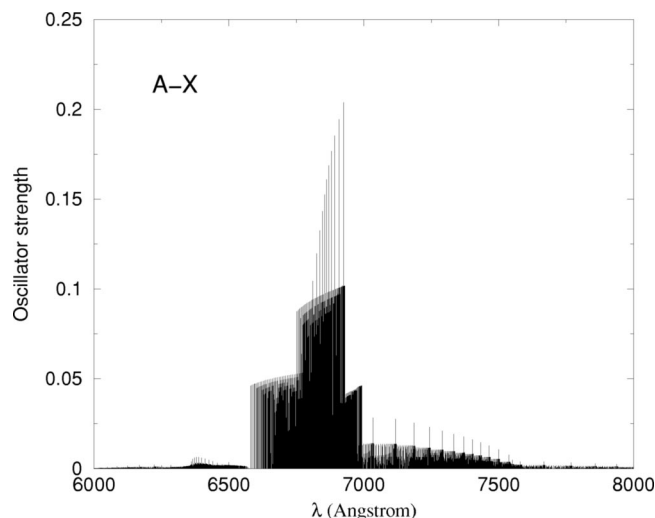


FIG. 3. Absorption oscillator strengths for vibration-rotation transitions for $A^2\Pi \leftarrow X^2\Sigma^+$.

the wavelength of the absorbed photon. The $A \leftarrow X$ oscillator strength distribution thus obtained is typical (cf. Ref. 26 for the $A \leftarrow X$ line list of MgH), with the predominance of diagonal vibrational transitions ($\Delta v = v' - v'' = 0$), decreasing as the vibrational number increases, over the central wavelength range. Transitions with $\Delta v = v' - v'' = +1$ and $\Delta v = v' - v'' = -1$ dominate at shorter and longer wavelength values, respectively. The series of peaks arising from the $N' = 1 \leftarrow N'' = 0$ lines of the R branch [$R(0)$] has intensities larger by a factor 2 than all other lines in the same wavelength region, because neither a Q -branch nor a P -branch transition is allowed for $N'' = 0$. An examination of the wavelength distribution of the lines shows that, apart from these peaks, the R -branch ($\Delta N = N' - N'' = +1$) contribution dominates over the wavelength range 6580–6750 Å. Other lines observed in Fig. 3 are to be assigned mainly to the Q -branch transitions ($N' = N''$), which are about two times more intense than the R and P branches over the whole considered wavelength range. Nevertheless, the P branch ($\Delta N = N' - N'' = -1$) appears to play a major role over the wavelength ranges 6430–6580 Å and 6930–7000 Å. The band-head is at 6930 Å, somewhat longer wavelength than corresponding bandhead for MgH at 5187 Å.

The rotational oscillator strengths corresponding to the $B/B' \leftarrow X^2\Sigma^+$ are plotted as a function of the absorbed photon wavelength in Fig. 4. As in the $A \leftarrow X$ case, the oscillator strength distribution is strongest for the R -branch transitions, as can be seen over the range 5820–6400 Å, where transitions to $v' = 0$ of the $B/B' \leftarrow X^2\Sigma^+$ dominate. Out of that range, the P branch contributes with almost the same intensity as the R branch. Moreover, there exists significant oscillator strength in the near-infrared region. Our calculations show that the most intense peaks depicted in that region are to be attributed mainly to R and P transitions between high-lying rotational states of the $v' = 0$ and the topmost rotational levels of the $v'' = 4-9$ vibrational states of the $X^2\Sigma^+$ electronic state. Transitions to the only vibrational level of the B' well, $v' = 4$, produce noticeable contributions to the oscillator strength distribution both in the red and near-

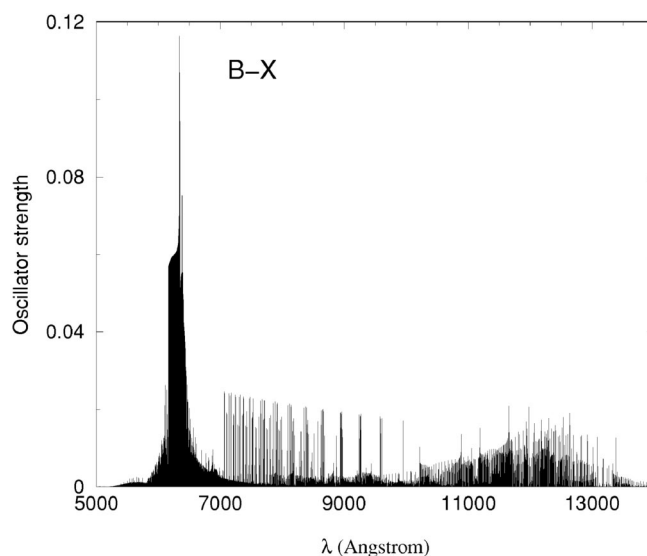


FIG. 4. Absorption oscillator strengths for vibration-rotation transitions for $B/B' \leftarrow X^2\Sigma^+$.

infrared regions, with band heads near 6340, 6440, 10 210, 11 180, 12 240, and 13 340 Å.

As for the case of $A^2\Pi \leftarrow X^2\Sigma^+$ transition, the $E^2\Pi \leftarrow X^2\Sigma^+$ oscillator strength distribution presented in Fig. 5 is quite typical with respect to the relative intensity of the R , Q , and P branches.

In Figs. 6 and 7 are depicted the rotational line absorption oscillator strengths for transitions from the $X^2\Sigma^+$ to the $C^2\Sigma^+$ and $D^2\Sigma^+$ states, respectively. For the $C^2\Sigma^+ \leftarrow X^2\Sigma^+$ transition, the rotational oscillator strengths show a broad contribution over the wavelength range 3380–3540 Å, with a typical series of intense sharp peaks corresponding to the $R(N'' = 0)$ lines of the diagonal vibrational transitions. The absence of marked structures in the intensity distribution can be attributed to the use of a unit dipole transition moment function (Franck-Condon approximation) in this work. A plot of the band oscillator strengths given in Ref. 3 reveals

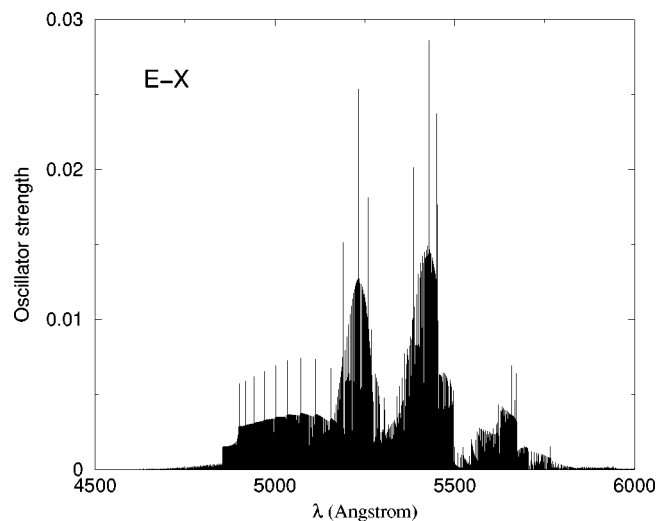


FIG. 5. Absorption oscillator strengths for vibration-rotation transitions for $E^2\Pi \leftarrow X^2\Sigma^+$.

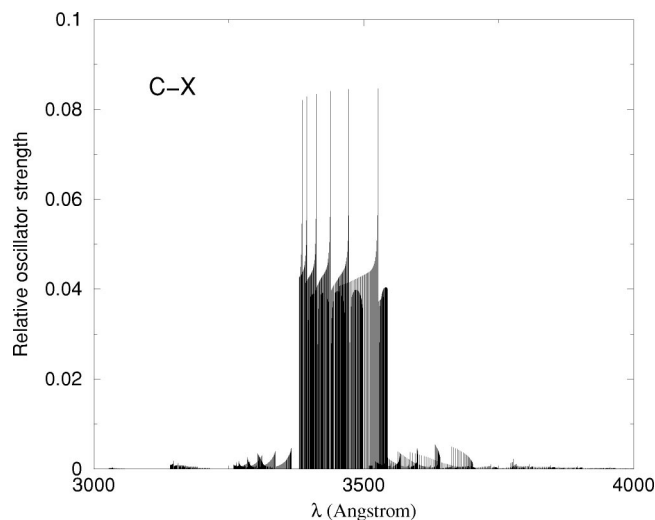


FIG. 6. Absorption oscillator strengths for vibration-rotation transitions for $C^2\Sigma^+ \leftarrow X^2\Sigma^+$ (relative intensity scale).

a similar wavelength grouping of the transitions, though our oscillator strengths are somewhat weaker. Due to the lack of a dipole transition moment, the $C \leftarrow X$ line list computed here is highly uncertain and should be used with caution.

From the particular nature of the $D^2\Sigma^+$ electronic state, characterized by two avoided crossings, results a very complex oscillator strength distribution for the $D^2\Sigma^+ \leftarrow X^2\Sigma^+$ transition, with an anomalous intensity distribution of the $R(N''=0)$ peaks series which reach maximum values for nondiagonal vibrational transitions, as was noted by Leininger and Jeung.³ Comparison of our rotational oscillator strength plot to the band oscillator strength plot given in Ref. 3 suggests many similarities for $\lambda < 5500$ Å. However, we do not obtain the more intense transitions given in Ref. 3 for longer wavelengths, presumably due to our adjustments in the dipole transition moment. Leininger and Jeung³ find the largest band oscillator strength for the $\Delta v = v' - v'' = 9 - 13$ for which the matrix element overlap will be dominated by relatively large R , since their dipole transition moment func-

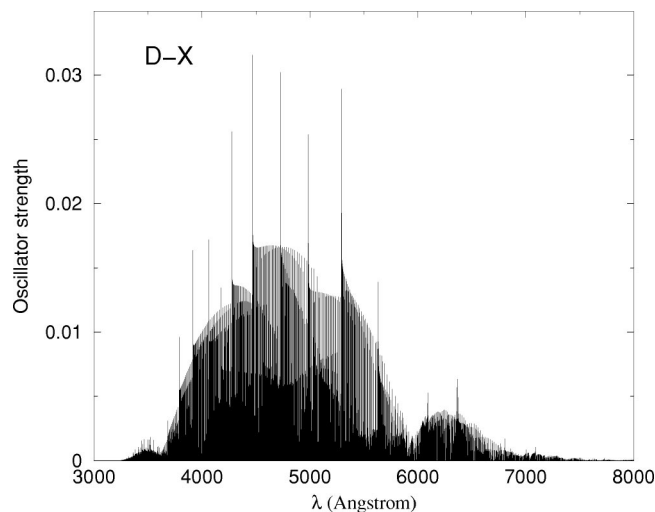


FIG. 7. Absorption oscillator strengths for vibration-rotation transitions for $D^2\Sigma^+ \leftarrow X^2\Sigma^+$.

tion is large in the separated-atom limit. However, we argued above that the dipole transition moment should vanish in the separated-atom limit. The uncertainties in the transition moment translate into considerable uncertainty in the $D \leftarrow X$ line list.

IV. CONCLUSION

Extensive and comprehensive absorption line lists have been generated for the transitions from the ground $X^2\Sigma^+$ state to the $A^2\Pi$, $B^2\Sigma^+$, and $E^2\Pi$ low-lying excited states of calcium hydride. The calculations are in good agreement with the available theoretical and experimental data for the vibrational energy levels and band oscillator strengths. The $B/B' \leftarrow X$ and the $D \leftarrow X$ transitions show complex intensity distributions resulting from perturbations due to the presence of avoided crossings. Oscillator strengths for the $D \leftarrow X$ transitions are highly uncertain due to the large uncertainty in the available dipole transition moment function. The Franck-Condon approximation has been used for the $C \leftarrow X$ transition for which *ab initio* calculations of the dipole transition moment function are lacking.

The most significant contributions to the overall CaH opacity arise from the $A \leftarrow X$ and $B/B' \leftarrow X$ transitions in the wavelength ranges 6600–7500 Å and 5800–7500 Å, respectively. The use of these new line lists in stellar and planetary atmosphere codes should significantly improve the description of the opacity of numerous cool stars where CaH is an important absorber.²

ACKNOWLEDGMENTS

This work was supported by NASA Grant No. NAG5-10551. P.F.W. is grateful to T. Leininger for providing the dipole transition moments, to G.-H. Jeung for useful discussions, and to R. J. Le Roy for the use of the LEVEL 7.5 code. We thank A. Schweitzer and P. H. Hauschildt for indicating to us the importance of CaH, and J. Hinze for helpful comments.

¹S. Sakamoto, G. J. White, K. Kawaguchi, M. Ohishi, K. S. Usuda, and T. Hasegawa, *Mon. Not. R. Astron. Soc.* **301**, 872 (1998).

²A. Burrows, W. B. Hubbard, J. I. Lunine, and J. Liebert, *Rev. Mod. Phys.* **73**, 719 (2001).

³T. Leininger and G.-H. Jeung, *J. Chem. Phys.* **103**, 3942 (1995).

⁴L. Klynning and H. Martin, *J. Phys. B* **14**, L365 (1981).

⁵H. Martin, *J. Mol. Spectrosc.* **108**, 66 (1984).

⁶H. Martin, *J. Chem. Phys.* **88**, 1797 (1988).

⁷G. Chambaud and B. Lévy, *J. Phys. B* **22**, 3155 (1989).

⁸A. Boutalib, J. P. Daudey, and M. El Mouhtadi, *Chem. Phys.* **167**, 111 (1992).

⁹R. Pereira, S. Skowronek, A. González Urena, A. Pardo, J. M. L. Poyato, and A. H. Pardo, *J. Mol. Spectrosc.* **212**, 17 (2002).

¹⁰K. P. Huber and G. Herzberg, *Molecular Spectra and Molecular Structure, Vol. IV, Constants of Diatomic Molecules* (Van Nostrand Reinhold, New York, 1979).

¹¹NIST Atomic Spectra Database (1999), http://aeldata.phy.nist.gov/cgi-bin/AtData/main_asd

¹²J. M. Standard and P. R. Certain, *J. Chem. Phys.* **83**, 3002 (1985).

¹³A. Dalgarno and A. E. Kingston, *Proc. Phys. Soc. A* **73**, 455 (1959).

¹⁴M. Merau, C. Tendo, and M. Rérat, *Chem. Phys. Lett.* **343**, 397 (2001).

¹⁵T. Leininger, Ph.D. thesis, Louis Pasteur University, Strasbourg, France (1996).

¹⁶R. P. Saxon, K. Kirby, and B. Liu, *J. Chem. Phys.* **69**, 5301 (1978).

¹⁷E. E. Whiting and R. W. Nicholls, *Astrophys. J., Suppl.* **27**, 1 (1974).

¹⁸M. Larsson, *Astron. Astrophys.* **128**, 291 (1983).

¹⁹J. W. Cooley, *Math. Comput.* **15**, 363 (1961).

²⁰R. J. Le Roy, LEVEL 7.5, University of Waterloo Chemical Physics Research Report CP-655 (2002). Source code and manual available at <http://leroy.uwaterloo.ca>

²¹B. Kaving and B. Lindgren, *Phys. Scr.* **24**, 752 (1981).

²²T. Gustavsson, L. Klynning, and B. Lindgren, *Phys. Scr.* **31**, 269 (1985).

²³C. Carlsund-Levin, N. Elander, A. Nunez, and A. Scrinzi, *Phys. Scr.* **65**, 306 (2002).

²⁴L. Klynning, H. Martin, P. Nylén, and P. Royen, *Phys. Scr.* **25**, 362 (1982).

²⁵The complete list of CaH rovibrational levels and oscillator strength data

is available online at the UGA Molecular Opacity Project database website <http://www.physast.uga.edu/ugamop/>. See EPAPS Document No. E-JCPSA6-118-002323 for tables of the above data and tables of the potential energy curves and dipole transition moment functions. A direct link to this document may be found in the online article's HTML reference section. The document may also be reached via the EPAPS homepage (<http://www.aip.org/pubservs/epaps.html>) or from <ftp.aip.org> in the directory /epaps/. See the EPAPS homepage for more information.

²⁶P. F. Weck, A. Schweitzer, P. C. Stancil, P. H. Hauschildt, and K. Kirby, *Astrophys. J.* **582**, 1059 (2003).

²⁷In atomic mass units, Aston's scale.